Theoretical search for possible Au-Si crystal structures using a genetic algorithm

Yue-Hang Dong, Wen-Cai Lu, Xin Xu, Xin Zhao, K. M. Ho, and C. Z. Wang

Phys. Rev. B **95**, 134109 — Published 18 April 2017

DOI: 10.1103/PhysRevB.95.134109

Theoretical search for possible Au-Si crystal structures using genetic algorithm

Yue-Hang Dong,[1,2] Wen-Cai Lu,[1,3,*] Xin Xu,[3] Xin Zhao,[4] K. M. Ho[4], C. Z. Wang[4,*]

[1]Institute of Theoretical Chemistry, Jilin University, Changchun, Jilin 130021, P. R. China

[2]School of Data Science and Software Engineering, Qingdao University, Qingdao, Shandong 266071, P. R. China

[3]College of Physics and Laboratory of Fiber Materials and Modern Textile, Growing Base for State Key Laboratory, Qingdao University, Qingdao, Shandong 266071, P. R. China

[4]Ames Laboratory – US DOE and Department of Physics and Astronomy, Iowa State University, Ames, Iowa 50011, USA

PACS number(s): 61.50.Ah, 61.66.Fn, 63.20.D-

Abstract:

We performed a global search for possible Au-Si crystal structures using genetic algorithm (GA) combined with density functional theory (DFT) calculations. Two Au-Si structures of Au_8Si_8 and $Au_{16}Si_8$ were found to be energetically stable and have no imaginary frequencies by phonon calculations. The formation energies of all the studied structures gave a convex hull of Au-Si system, showing that the most stable composition was Au-Si = 1:1, and the Si-rich structures were much less stable than the Au-rich ones.

*Corresponding authors. Emails: wencailu@jlu.edu.cn; wangcz@ameslab.gov

I. INTRODUCTION

Metal-semiconductor interaction is a subject of considerable interest with regard to both technical applications (e.g., metal-insulator-semiconductor (MIS) devices) and fundamental researches (e.g., Schottky barrier).[1,2] Au-Si system, as a typical example of metal-semiconductor alloy, has drawn considerable attention due to the deep eutectic region in such system. For instance, the melting point decreases to 363℃ for 81.0% Au,[3] as compared with melting temperatures 1064℃ and 1414℃ for pure Au and Si, respectively. In semiconductor industry, Au and Si are widely used in solder and making electrical contacts which can be used to form lifetime controller for electric-charge carriers in fast-switching devices and microchip packing and interconnection in micro-electromechanical systems (MEMS).[4-7] Moreover, in nanotechnology, Au-Si eutectic alloy is also of great interest for growing Si nanowires.[8]

While stable bulk crystalline Au-Si intermetallic compounds are hard to form,[9,10] Au–Si alloy was discovered as the first binary metallic glass-forming alloys.[11] By using the rapid quenching, a technique which has been known to produce meta-stable phases,[12] Au-Si amorphous alloy can be obtained from liquid Au-Si. Although the Au-Si amorphous alloy exhibits remarkable physical properties, the atomic structure and formation mechanism of amorphous alloys remain poorly understood.[10,13,14] Gold silicide structures at different compositions have also been an interesting subject of research and have attached a lot of investigations. Various experimental methods have been used such as evaporation, irradiation,[15-16] sputter deposition, blast-atomizing rapid quenching and X-ray-diffraction (XRD) to investigate the formation and structures of possible stable and metastable phases of gold silicide.[10,17,18] It has been reported that Au deposition on a Si substrate can lead to the formation of silicide even at room temperature. Si atoms diffuse from the Si substrate and cross through the Au overlayer to form an Au-Si thin film alloy on the Au surface.[19] Another observation is that a layer of Au_3Si_2 formed at the top of Au film when Au atoms were deposited on Si(111) at room temperature.[20] The structure of the eutectic liquid was experimentally

investigated via X-ray diffraction measurements in study.[18] By using glancing angle X-ray diffraction, Shpyrko et al. discovered a crystalline monolayer on top of eutectic liquid of $Au_{82}Si_{18}$ under the temperature higher than the alloy's melting point.[10] However, none of the experimental studies mentioned above provided detailed structure information about the observed alloy phases due to the complexity of Au-Si alloys.[10,17,20-22] Resolving the structures of complex alloys experimentally is still very difficult, which impedes the understanding and further optimization of the alloys for applications.[23] On the other hand, computational algorithms and methods for *ab initio* structure prediction can speed up the investigation of the structures of Au-Si alloy.[24,25] Pasturel et al. investigated Au-Si system via *ab initio* molecular dynamics (AIMD) simulations,[26] and revealed that Au and Si atoms are very reactive with each other,[13,27] and lead to strong intermixing between Si and Au atoms.[26] By first-principles electronic structure calculations, Tasci et al. predicted a new ground-state of crystalline Au_4Si in spite of no Au-Si compounds have been shown in the existing phase diagram.[28] Lee et al. examined the atomic structures, energetics, and the bonding of amorphous Au-Si alloys.[13] They also studied the surface segregation behavior of Si in amorphous Au-Si alloys using AIMD.[27] Lee's results predicted that stable structure of Au-Si alloys can be formed when the Si content is around 40–50%, with an energy gain about 0.15 eV/atom.

In this paper, we applied the genetic algorithm (GA) to search for possible stable crystal structures of Au-Si compounds. Our studies predict several new stable Au-Si compounds. The dynamical stability and the electronic properties of these new compounds were also studied by first-principles calculations. The predictions from our theoretical studies would provide useful guidance for experimental synthesis and discovery of new compounds for Au-Si systems.

II. METHOD

Applications of GA to perform the global optimization to search for the stable

atomic structures of clusters and crystals have been rapidly developed recently due to the advances of the computer power and computational software. The adaptive Genetic Algorithm code[30,31] (AGA) used in this work is based on real space cut-and-paste operations[29] and has been successfully applied to predictions of many complex crystal structures,[23,32] such as the atomic structure of a rare-earth (RE) free permanent magnetic material – Zr_2Co_{11},[23] and the layered structures of thin film solar cell materials - Cu_2Te and Cu_2Se.[32] In the present study, we performed a systematic GA search for Au-Si crystal structure using first-principles calculations as the energy evaluation method. The GA searches were performed without any pre-assumptions on the type of Bravais lattice, the atom basis, or the unit cell dimensions. The chemical compositions were the only given information, and the initial atomic positions in the unit cells were randomly generated.

Considering pure Au conventional cell is a face centered cubic (FCC) structure (#225, Fm-3m) with 4 atoms, while pure Si conventional cell is a diamond structure (#227, Fd-3m) with 8 atoms, our searching therefore started from cells with 8 atoms which is their least common multiple, such as Au_7Si, Au_6Si_2, Au_5Si_3, Au_4Si_4, Au_3Si_5, Au_2Si_6 and $AuSi_7$. We also considered the cells of similar size with varied number of atoms in the unit cell from 7 to 12 to cover some special compositions that were mentioned in the literature, such as Au_4Si,[28] Au_2Si,[21,42] Au_3Si_2,[20] $AuSi_2$ and Au_4Si_3.[10,21] The searches were performed for unit cells with 4 ~ 6 up to 16 ~ 24 atoms, and a population of 32 (64) structures were used for unit cells containing up to 12 (24) atoms. Each GA search was considered to be converged after the lowest energy in the population remains unchanged in 200 steps. The low-energy structures of these 12 compositions were collected from GA searches for finer structure optimization.

The first-principles calculations were performed using density functional theory (DFT) within generalized-gradient approximation (GGA) with projector-augmented wave (PAW) pseudopotential method by VASP code.[33-36] The GGA exchange-correlation energy functional parameterized by Perdew, Burke, and Ernzerhof (PBE) was used.[37] The kinetic energy cutoff for the plane-wave basis set was 360 eV and the Monkhorst-Pack's scheme was used for Brillouin zone

sampling.[38] A k-point mesh of 4 × 4 × 4 was employed during the GA searches. Much denser k-point meshes as listed in TABLE I were used to refine the structures selected from GA search in order to determine the ground-state structures. The electronic band structures, density of states (DOS) and Bader charge analysis were also performed for the low-energy structures selected from GA search.[39] The phonon dispersion spectra were also calculated by the supercell method implemented in Phonopy code,[40] using the same exchange and correlation functional as in the total energy calculations, and a kinetic energy cutoff of 500 eV.

To investigate the energetic stability of structures at different compositions obtained from GA search, we calculated the formation energy (E_f) of the compound structures using the following definition:

$$E_f(\mathrm{Au}_m\mathrm{Si}_n) = [\mathrm{E}(\mathrm{Au}_m\mathrm{Si}_n) - \mathrm{m}\times E(\mathrm{Au}) - \mathrm{n}\times \mathrm{E}(\mathrm{Si})] / (\mathrm{m}+\mathrm{n})$$

where *m* and *n* stand for the numbers of Au atom and Si atom, respectively, and E(Au) and E(Si) are the energies (per atom) of FCC Au and diamond Si crystalline structures, respectively. As listed in TABLE I, the calculations for the FCC Au and diamond Si structures were also performed with denser k-points, and the calculations gave accurate results for the formation energy using both conventional unit cells and their primitive cells.

III. RESULTS AND DISCUSSES

From GA search, we found many low-energy crystal structures with similar formation energies. The energies of the lowest-energy structures and some of the second best structures we found from all the 12 compositions were plotted in Fig. 1, where blue solid squares marked the lowest-energy ones and purple triangle represented the second best ones. We noticed that negative formation energies occur at 4 compositions of 50.0%, 66.7%, 75.0% and 80.0% Au contents, respectively, indicating that the compounds at these 4 compositions are stable against segregation

into pure Si and Au crystals.

In Hoshino and Tasci's work,[20,28] 11 relative stable Au-Si compounds were predicted, 9 of them were rich of gold, consistent with our convex hull (Fig. 1), in which, the most stable structures are also Au-rich. In our prediction, the most stable one is of composition 50.0% of Au content, this also agrees with the results from literature,[13] which suggested that the stable Au-Si alloy should be around Au content 50.0% to 60.0%.

In the following, we are going to discuss structures at the 4 stable compositions in more detail. The structures at other compositions will also be briefly discussed. Some key information about these structures are listed in TABLE II.

A. Structures of Au-Si = 1:1

The lowest-energy structure we found of this composition is Au_8Si_8, shown in Fig. 2. It belongs to space group of #63 Cmcm, and its conventional unit cell contains 16 atoms, while 8 for its primitive cell. The primitive cell is marked by the red rhombus in Fig. 2 (a), and the conventional unit cell is the black rectangle in Fig. 2 (a) and Fig. 2 (b). Compared with Au_8Si_8, another structure Au_4Si_4 as shown in Fig. 3 is of the same composition but relatively higher in energy, and belongs to space group #59 Pmmn. Lattice system of these two structures is orthorhombic.

The lattice parameters of the Au_8Si_8 are a = 8.275 Å, b = 9.317 Å, c = 4.751 Å, $\alpha = \beta = \gamma = 90^o$, respectively, its primitive lattice parameters are a = b = 6.227 Å, $\alpha = \beta = 90^o$, $\gamma = 83.06^o$, and two different 8g Wyckoff positions are occupied as Au (0.78761, 0.17110, 0.25000) and Si (0.85535, 0.91212, 0.25000), respectively. The lattice parameters of the structure Au_4Si_4 in Fig. 3 are a = 4.725 Å, b = 6.794 Å, c = 4.875 Å, $\alpha = \beta = \gamma = 90^o$, the basis Au and Si atoms occupy 2 different 4e Wyckoff positions: Au (0.00000, 0.23143, 0.83688) and Si (0.50000, 0.17532, 0.65236). The formation energy E_f of the structure Au_8Si_8 is -51.11 meV/atom and that of structure Au_4Si_4 is -41.94 meV/atom. Both structures exhibit layer motif which can be better viewed from the lattice vector **a** in Au_8Si_8 and from the lattice vector **c** in Au_4Si_4. As

shown in Fig. 2 (a), along the lattice vector **a**, the Au_8Si_8 structure shows an ABAB alternative layered arrangement. The distance between the layers is 2.3754 Å. This structure consists of two types Si-terminated Au_2Si_2 chains tilted about 41.6˚ with respect to the direction of the lattice vector **b**, as marked by the green rectangular in Fig. 2 (a). These two type chains form two adjacent zigzag ribbons with a dislocation distance along the direction of the lattice vector **b**. The top view (along vector **c**) of layer A and B were shown in Fig. 2 (c) and Fig. 2 (d), respectively, and we found that these two layers are rotationally – symmetric, in other words, layer A can turn into layer B by just rotating 180° along the lattice vector **c**. On the other hand, the atomic arrangement in the structure of Au_4Si_4 is also formed layer by layer, the distance between the layers decreases to 2.3624 Å. The top view was given in Fig. 3 (a), and the side view in Fig. 3 (b). We found Si-terminated Au_2Si_2 chains again as marked in green rectangles. The tilting angle of the chains in this structure is 55.2˚, larger than that in the structure of Au_8Si_8.

B. Crystal structures of Au-Si = 4:1

Au-Si=4:1 composition system is quite close to the composition of Au-Si eutectic, which is 81% Au content. The two low-energy structures found at this composition are shown in Fig. 4, both have negative formation energies.

The lowest-energy structure is I-42m #121 Au_8Si_2 as shown in Figs. 4 (a) and (b), it has 10 atoms in a tetragonal cell. This structure type is the same as CI_4 which reported by Pohl et al.[41] Its optimized lattice parameters are: a = b = 5.761 Å, c = 5.549 Å, $\alpha = \beta = \gamma = 90^o$. The Au atom at (0.29486, 0.29486, 0.3377) is located at the 8i Wyckoff position, while Si atom occupies the 2b Wyckoff position: Si (0.0, 0.0, 0.5). The structure Au_8Si_2 possesses a rather ordered cross "X" character shown clearly in its top view in Fig. 4 (a). We can see two types of Au_2Si chain, marked by the green rectangular in Fig. 4 (a), tilted about 45˚ with respect to the direction of the lattice vector **b**. The Si atom marked in a red circle is shared by two type of Au_2Si chains. As shown in Fig. 4 (b), the green octagon outlines a basic repeat unit, with 8 Au atoms on the edges and one Si atom is located at the center. Tilted about 44.4˚

with respect to the lattice vector **b**. Figs. 4 (c) and (d) shows the second lowest-energy structure of this composition. The unit cell of this structure ($Au_{16}Si_4$) is orthothombic and belongs to the space group $C222_1$ #20. The lattice parameters are a = 7.881 Å, b = 5.977 Å, and c = 7.928 Å, and the Wyckoff positions of Au atoms are 8c (0.17959, 0.21212, 0.24212) and 8c (0.50043, 0.27266, 0.07267), and the Si atom is at 4a (0.7264, 0, 0). From Fig. 4 (c), it can be seen that the atoms are clearly ordered in an ABCDABCD-stacked multi-layer form, each layer contains the same type of atoms. The similar multi-layer appearance can be seen from the side view in Fig. 4 (d), but the layers are stacked in an ABAB form.

Comparing the I-42m Au_8Si_2 and $C222_1$ $Au_{16}Si_4$ structures with the Au_4Si structure reported by Tasci et al.,[28] we found that, although they have similar appearance, their space groups are different, i.e., it is p-421c #114 for the Au_4Si structure in Ref. 28, while I-42m and $C222_1$ for Au_8Si_2 and $Au_{16}Si_4$, respectively, in present work. We also compared their formation energies under the same input parameters and system configurations. The E_fs of the GA predicted Au_8Si_2 (-29.23 meV/atom) and $Au_{16}Si_4$ (-28.02 meV/atom) are lower than -16.68 meV/atom of the Au_4Si in Ref. 28.

In addition, we generated their simulated XRD patterns, and compared them with experimental XRD images. The major peaks of the $C222_1$ $Au_{16}Si_4$ are close to the experimental data of $Au_{76.7}Si_{23.3}$,[17] but different indexed (see the supplementary file).[47]

C. Structures of Au-Si = 2:1

Fig. 5 shows the structure of $Au_{16}Si_8$ which is the lowest-energy structure we found at this composition. The unit cell was drawn by black rectangle in Fig. 5 (a). The cell type is orthorhombic and of the space group $C222_1$ #20. The parameters of the unit cell are: a = 7.508 Å， b = 7.254 Å， c = 9.093 Å， $\alpha = \beta = \gamma = 90°$, and the atom number is 24. The Au atoms occupy two 8c Wyckoff positions: Au1 (0.95211, 0.17066, 0.89139) and Au2 (0.95211, 0.17066, 0.89139), the Si atoms occupy one 8c Wyckoff position: Si (0.16823, 0.29256, 0.32582). In addition, the primitive cell of

this structure has 12 atoms, and the lattice parameters are: a = b = 5.219 Å， c = 9.093 Å, α = β = 90°, γ = 88.02°. The formation energy of this structure is -32.53 meV/atom. The top view of $Au_{16}Si_8$ in Fig. 5 (a) shows a layered form. The two type of basic repeat units in a single layer are highlighted within green rectangles. The average distance between each layer is about 3.627 Å. Fig. 5 (b) is the side view, which presents a ABAB multi-layered motif. The layer features as marked in green lines are connected in zigzag form. The Wyckoff positions of Au1, Au2 and Si were shown in Figs. 5 (c) and (d), where the Au2 atoms are represented by "+" marked yellow spheres. It is measured that the nearest distance from Au1 to atom Si is 2.426 Å, and 2.536 Å from atom Au2 to atom Si.

The second lowest-energy structure at this composition is Au_8Si_4, as shown in Fig. 6. It belongs to the space group $Pna2_1$ #33. The unit cell parameters are a = 8.400 Å, b = 5.948 Å, c = 4.552 Å, and α = β = γ = 90°. In this structure, the Au atoms occupy 4a Wyckoff positions: Au1 (0.89769, 0.94935, 0.00777) and Au2 (0.90514, 0.41378, 0.78663), the Si atoms occupy one 4a Wyckoff position, Si (0.15188, 0.22726, 0.01964). The formation energy of this structure is -21.11 meV/atom. Figs. 6 (a) and (b) are top and side view of the Au_8Si_4 structure. A double layered feature can be seen, and the distance between the layers is about 2.1 Å.

D. Structures of Au-Si = 3:1

In the Au-Si = 3:1 composition (75% of Au content), the result of our search gave a triclinic structure Au_6Si_2 shown in Fig. 8 (a). Its unit cell parameters are a = 4.752 Å, b = 6.967 Å, c = 4.839 Å, α = 75.563°, β = 74.512°, and γ = 79.107°. Its formation energy is -24.50 meV/atom which is lower than the FCC Au_3Si reported in Bisit's study.[43] However, the phonon calculation shows that it is not a dynamically stable structure. As we can see from Fig. 1, the E_f is located at the local energy maximum although it has a negative formation energy. Also, we compared the simulated XRD and experimental XRD image. The main peaks of the Au_6Si_2 are close to the experimental data of Au_3Si,[22] but small peaks have deviations (see the supplementary file).[47]

E. Structures at other compositions

In Fig. 1, we noticed that the formation energies of Au_2Si_4 (33.3% Au), Au_6Si_4 (60% Au), Au_5Si_3 (62.5% Au) and Au_7Si (87.5% Au) are positive but less than 20 meV/atom above the line connecting the energies of pure Au and Si crystals. These structures might be formed at high temperature or non-equilibrium synthesis conditions. It is therefore worthwhile to briefly discuss the atomic structures of these compounds. The lowest-energy optimized structures we found from our GA search at these compositions are shown in Figs. 7 (a-d).

We note that the structure at the composition 60% Au has the energy located in a local minimum point in our convex hull (Fig. 1). This agrees with the Hoshino's study,[20] in which a Au_3Si_2 surface crystalline phase were found on-top of liquid Au-Si alloy. The structure we optimized at this composition is Au_6Si_4 shown in Fig. 7 (a).

Surface crystalline phases were also reported in the experimental studies at composition 33.3% and 66.7% Au.[10,21] Another study reported that a spherical bulk-like crystal structure, which is the first Si-rich Au-Si alloy with 33.3% of the Au content, can be observed after annealing.[42] In our present study, we found that the energy of the structure at 33.3% Au (i.e., Au_2Si_4) from our GA search is located in a deep minimum in the convex hull (Fig. 1). Although the formation energy of this structure is positive, it is within 20 meV/atom above the line connecting the energies of pure Au and Si crystals. These results are consistent with the experimental observation on the formation of metastable phases at the composition of 33.3% Au.[10] The structure of Au_2Si_4 from our GA search is shown in Fig. 7 (d).

Finally, for the 12.5% Au composition, the lowest-energy structure $AuSi_7$ obtained from our GA search was shown in Fig. 8 (b). This structure belongs to the space group P-4m2 #115, and contains 8 atoms within its tetragonal unit cell. Atomic arrangement of its unit cell is almost the same as diamond silicon.

F. Dynamical stability and electronic structures

Besides the static energetic studies presented above, we performed phonon

calculations for the low-energy structures to investigate their dynamical stability. The phonon spectra of 50.0% (Au_8Si_8), 66.7% ($Au_{16}Si_8$) and 80.0% (Au_8Si_2 and $Au_{16}Si_4$) at Au composition were plotted in Fig. 9, showing that structure Au_8Si_8, $Au_{16}Si_8$, Au_8Si_2 and $Au_{16}Si_4$ are dynamically stable without any soft phonon mode. In addition, we have performed elastic constant calculations to investigate the mechanical stability of the predicted structures, and found that these four structures meet the mechanical stability criteria.[44] We thus assumed that the Cmcm Au_8Si_8, $C222_1$ $Au_{16}Si_8$, I-42m Au_8Si_2 and $C222_1$ $Au_{16}Si_4$ could be expected to be energetically, dynamically and mechanically stable.

We have also investigated the electronic properties of the newly found low-energy structures by performing band structure, density of states and Bader charge calculations.[39] The Bader charges of Au and Si of 4 structures were listed in TABLE III. Negative value indicates excess electron charge with respect to the neutral atom charge. We can see that most of the structures, except for the structure $C222_1$ $Au_{16}Si_4$, Au presents a negative value while Si presents a positive one, such kind of electron distribution may lead to the particular properties in Au-rich gold silicides. Also, all the three structures have no band gaps at the Fermi level, around where the density of states is also relatively small (Fig. 10), which is in agreement with that the Au-rich gold silicide may show more metallic properties.

IV. SUMMARY

In summary, we searched for possible Au-Si crystal structures at different compositions, and analyzed the tendency of stabilization of different compositions for gold silicide crystals. The calculations were performed by using the GA method combined with DFT calculations. We found that the newly predicted structures Au_8Si_8, $Au_{16}Si_8$, Au_8Si_2 and $Au_{16}Si_4$ are not only energetically stable but also dynamically stable. From our calculations, we noticed that the Si-rich Au-Si compounds may not exist under normal circumstances and thus the silicon tends to easily segregate out,[27] or penetrate to surface.[19] Moreover, the certain stable states may not likely to be the compositions with too much gold. In other words, metal-rich phases may also tend to

fit to new stable states under certain conditions (chemical, thermal, or physical), and this tendency can even cause the movement of nano-droplets.[45] This may enhance the rationality of our convex hull (Fig. 1), which suggests that the relative stable compositions of Au-Si crystal structures may locate from 50% up to 80% at the Au content, and the per atom formation energy E_f will raise up drastically when Au content is more than 80%.

ACKNOWLEDGMENTS

This work was supported by the National Natural Science Foundation of China (Grant No. 21273122). This work was also supported by the U.S. Department of Energy (DOE), Office of Science, Basic Energy Sciences, Materials Science and Engineering Division including a grant of computer time at the National Energy Research Scientific Computing Centre (NERSC) in Berkeley, CA. Ames Laboratory is operated for the U.S. DOE by Iowa State University under contract # DE-AC02-07CH11358.

References:

[1]L. Hultman, A. Robertsson, H. T. G. Hentzell, I. Engström, and P. A. Psaras, J. Appl. Phys. 62, 3647 (1987).

[2]A. K. Green and E. Bauer, J. Appl. Phys. 52, 5098 (1981).

[3]T. B. Massalski, Binary Alloy Phase Diagrams, 2nd ed. (American Society for Metals International, Materials Park, Ohio, 1990), p. 428.

[4]N. A. Stolwijk, B. Schuster, and J. Hölzl, Appl. Phys. A. 33, 133-140 (1984).

[5]E. Ö. Sveinbjörnsson, O. Engström, and U. Södervall, J. Appl. Phys. 73, 7311 (1993).

[6]J. Haubert, N. A. Stolwijkts, L. Tapferll, H. Mehrer, and W. Frank, J. Phys. C: Solid State Phys. 19, 5817-5836 (1986).

[7]J. S. Lin, C. C. Chen, E. W. G. Diau, and T. F. Liu, J. Mater. Process. Tech. 206, 425-430 (2008).

[8]J. B. Hannon, S. Kodambaka, F. M. Ross, and R. M. Tromp, Nature. 440, 69-71 (2006).

[9]N. Ferralis, R. Maboudian, and C. Carraro, J. Am. Chem. Soc. 130, 2681-2685 (2008).

[10]Oleg G. Shpyrko et al. Science. 313, 77-80 (2006).

[11]W. Klement, R. H. Willens, and Pol Duwez, Nature. 187, 869-870 (1960).

[12]D. M. Herlach, P. K. Galenko, and D. Holland-Moritz, Metastable Solids from Undercooled Melts (Elsevier, Amsterdam, 2007).

[13]S. H. Lee and G. S. Hwanga, J. Chem. Phys. 127, 224710 (2007).

[14]J. Maddox, Nature. 335, 201-201 (1988).

[15]S. Kumar, P. K. Sahoo, R. S. Chauhan, D. Kabiraj, U. Tiwari, D. Varma, and D. K. Avasthi, Nucl. Instr. and Meth. in Phys. Res. B. 212, 238-241 (2003).

[16]R. Khalfaoui, C. Benazzouz, A. Guittoum, N. Tabet, and S. Tobbeche, Vacuum. 81, 45-48 (2006).

[17]R. C. Krutenat, J. K. Tien, and D. E. Fornwalt, Metall. Metall. Trans. 2, 1479-1481 (1971).

[18]H. Fujii, S. Tahara, Y. Kato, S. Kohara, M. Itou, Y. Kawakita, and S. I. Takeda, J. Non-Cryst. Solids. 353, 2094-2098 (2007).

[19]A. Hiraki, E. Lugujjo, and J. W. Mayer, J. Appl. Phys. 43, 3643 (1972).

[20]Y. Hoshino, Y. Kitsudo, M. Iwami, and Y. Kido, Surf. Sci. 602, 2089-2095 (2008).

[21]Oleg G. Shpyrko *et al.*, Phys. Rev. B. 76, 245436 (2007).

[22]G.A. Andersen, J. L. Bestel, A. A. Johnson, and B. Post, Mater. Sci. Eng. 7, 83-90 (1971).

[23]X. Zhao, M. C. Nguyen, C. Z. Wang, and K. M. Ho, et al. Phys. Rev. Lett. 112, 045502 (2014).

[24]B. Meredig and C. Wolverton, Nat. Mater. 12, 123-127 (2013).

[25]S. Curtarolo, G. L.W. Hart, M. B. Nardelli, N. Mingo, S. Sanvito, and O. Levy, Nat. Mater. 12, 191-201 (2013).

[26]A. Pasturel, E. S. Tasci, M. H. F. Sluiter, and N. Jakse, Phys. Rev. B. 81, 140202 (2010).

[27]S. H. Lee, J. A. Stephens, and G. S. Hwang, J. Phys. Chem. C. 114, 3037–3041 (2010).

[28]E. S. Tasci, M. H. F. Sluiter, A. Pasturel, and P. Villars, Acta. Materialia. 58, 449-456 (2010).

[29]D. M. Deaven and K. M. Ho, Phys. Rev. Lett. 75, 288-291 (1995).

[30]M. Ji, K. Umemoto, C. Z. Wang, K. M. Ho, and R. M. Wentzcovitch, Phys. Rev. B. 84, 220105 (2011).

[31]S. Q. Wu, M. Ji, C. Z. Wang, M. C. Nguyen, X. Zhao, K. Umemoto, R. M. Wentzcovitch, and K. M. Ho, J. Phys.: Condens. Matter. 26, 035402 (2014).

[32]M. C. Nguyen, J. H. Choi, X. Zhao, C. Z. Wang, Z. Y. Zhang, and K. M. Ho, Phys. Rev. Lett. 111, 165502 (2013).

[33]P. E. Blochl, Phys. Rev. B. 50, 17953 (1994).

[34]G. Kresse and D. Joubert, Phys. Rev. B. 59, 1758 (1999).

[35]G. Kresse and J. Furthmüller, Comput. Mater. Sci. 6, 15 (1996).

[36]G. Kresse and J. Furthmüller, Phys. Rev. B. 54, 11169 (1996).

[37]J. P. Perdew, K. Burke, and M. Ernzerhof, Phys. Rev. Lett. 77, 3865 (1996).

[38]H. J. Monkhorst and J. D. Pack, Phys. Rev. B. 13, 5188 (1976).

[39]G. Henkelman, A. Arnaldsson, and H. Jónsson, Comput. Mater. Sci. 36, 254-360 (2006).

[40]Atsushi Togo and Isao Tanaka, Scr. Mater. 108, 1-1-5 (2015)

[42]F. H. Baumann and W. Schröter, Phys. Rev. B. 43, 6510 (1991).

[43]O. Bisit, C. Calandra, L. Braicovich, I. Abbati, G. Rossi, I. Lindau, and W. E. Spicer, J. Phys. C: Solid State Phys. 15, 4707-4716 (1982).

[44]J. F. Nye, Physical Properties of Crystals (Oxford University Press, Oxford, 1985).

[45]Curiotto S, Leroy F, Cheynis F, and Müller P, Surface Science. 632, 1-8 (2015).

[46]K. Momma and F. Izumi, J. Appl. Crystallogr. 44, 1272 (2011).

[47]See Supplemental Material at [URL will be inserted by publisher] for comparison of XRD patterns and information of another proposed Au_8Si_2 structure .

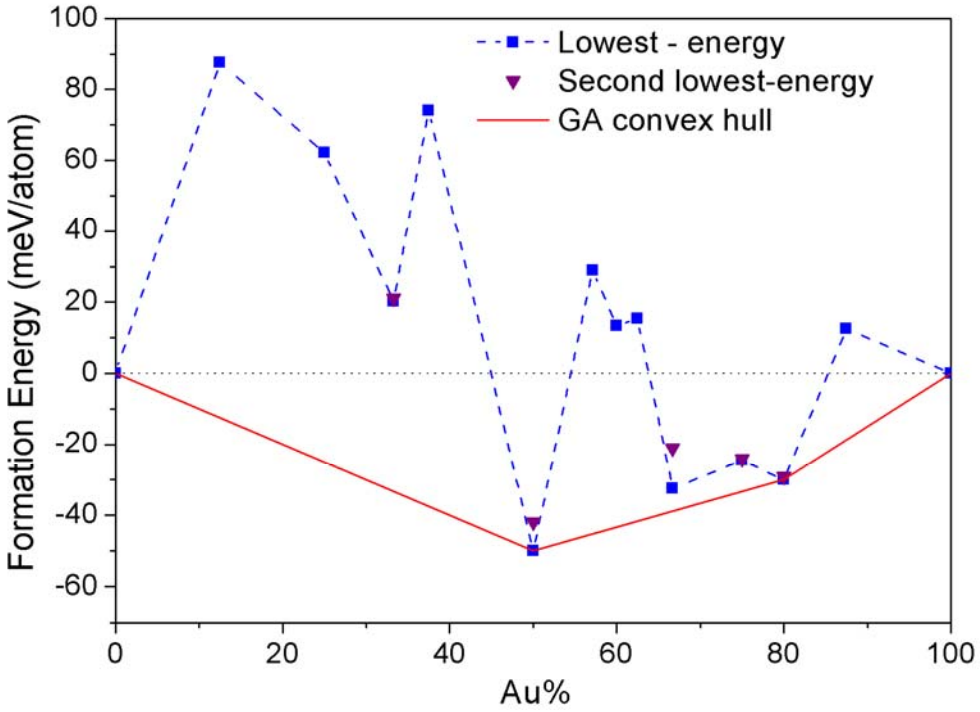

FIG. 1. Formation energies (E_fs) of the predicted Au-Si structures at various Au contents. The blue square and purple triangles represent the lowest-energy and the second lowest-energy structures, respectively.

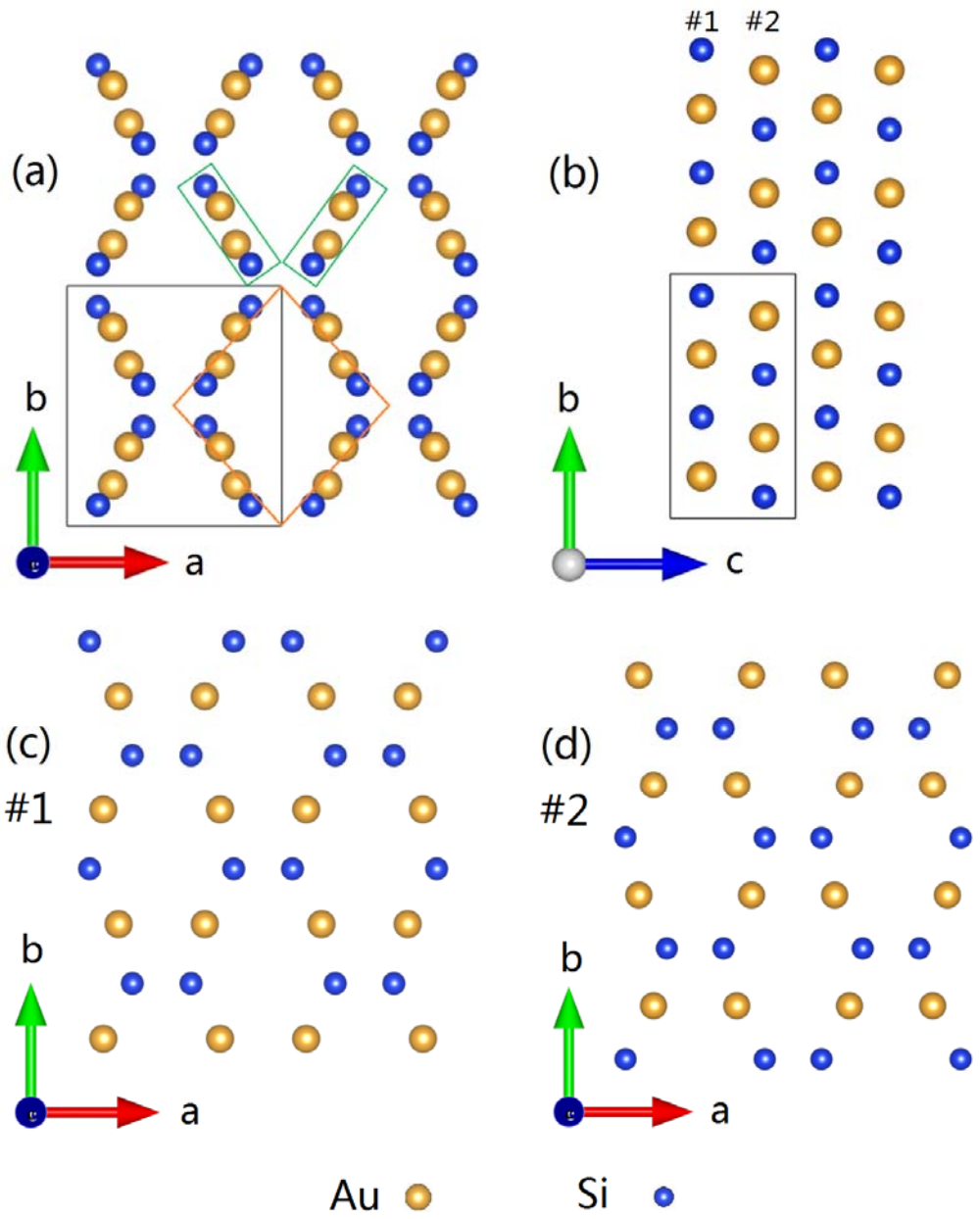

FIG. 2. Lowest-energy structure of Au_8Si_8, plotted by VESTA.[46] (a) and (b) Top and side views of the Au_8Si_8 structure; (c) and (d) top view of layer #1 and #2.

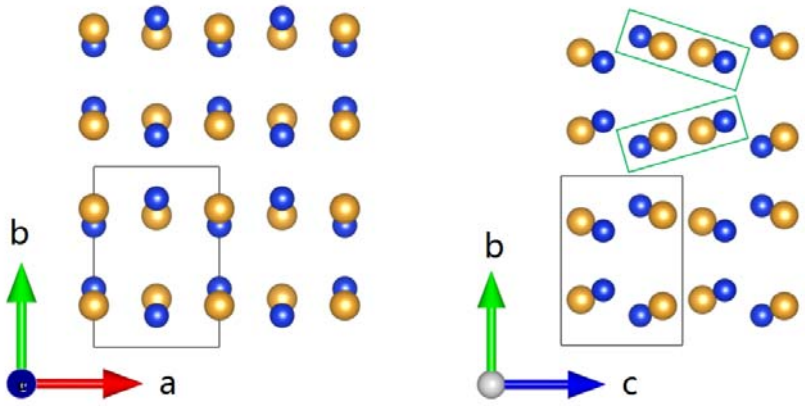

FIG. 3. Top and side views of the low-energy structure of Au_4Si_4, plotted by VESTA.[46]

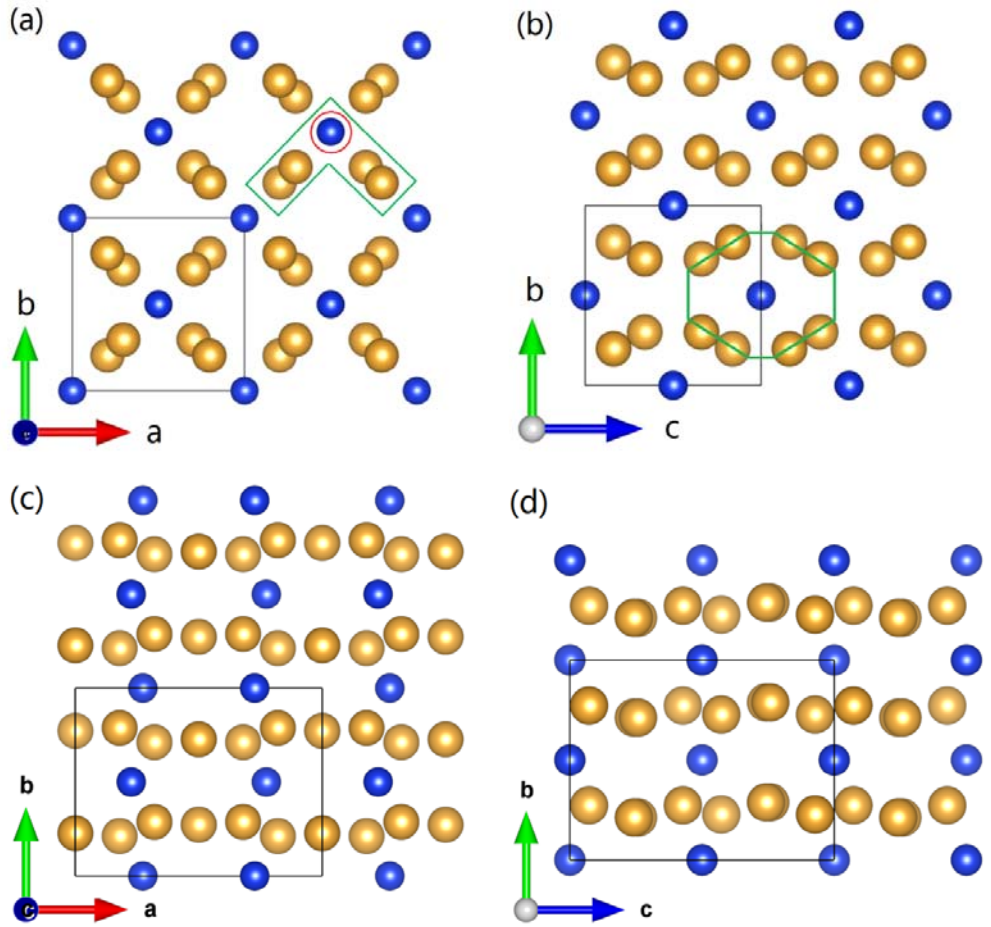

FIG. 4. Low-energy structures of Au_8Si_2 and $Au_{16}Si_4$, plotted by VESTA.[46] (a) and (b) Top and side views of the Au_8Si_2 structure. (c) and (d) Top and side views of the $Au_{16}Si_4$ structure.

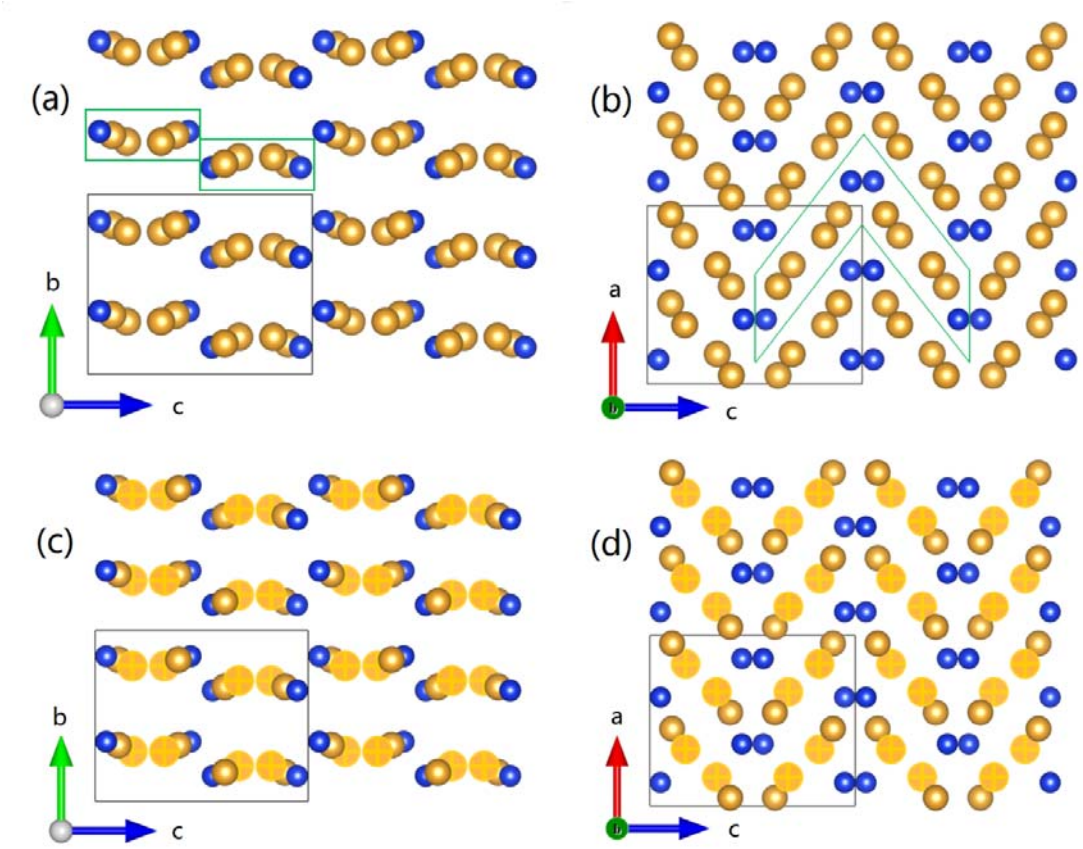

FIG. 5. Lowest-energy structure of $Au_{16}Si_8$, plotted by VESTA.[46] (a) and (b) Top and side views of $Au_{16}Si_8$; (c) and (d) top and side views of $Au_{16}Si_8$ with normal Au atoms and cross marked Au atoms, which indicates two different 8c Wyckoff positions.

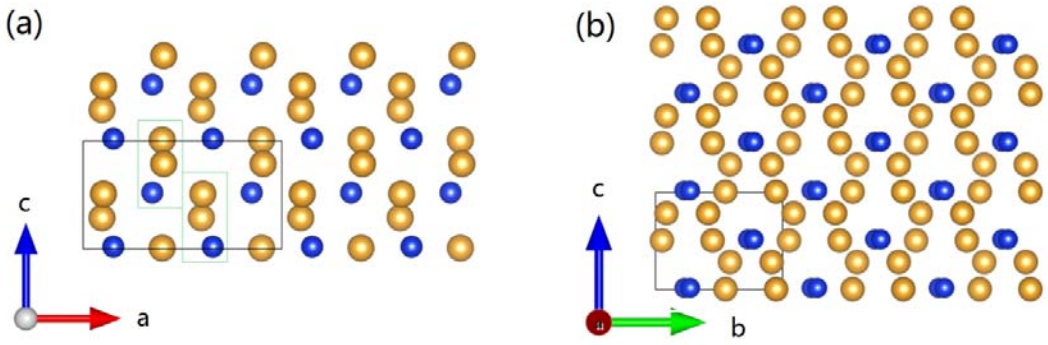

FIG. 6. Lowest-energy structure of Au_8Si_4, plotted by VESTA.[46]

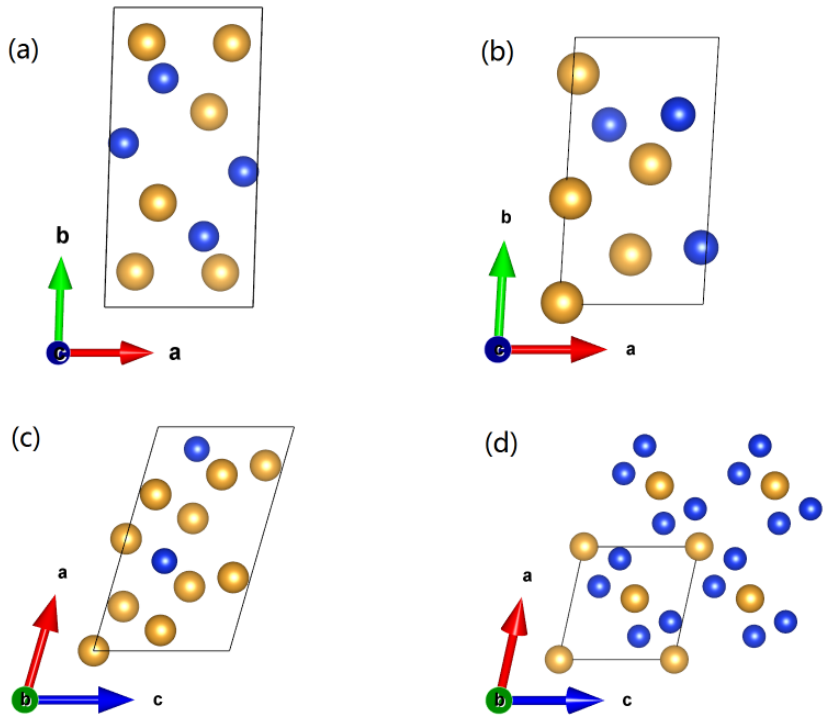

FIG. 7. Lowest-energy structures of (a) Au_6Si_4, (b) Au_5Si_3, (c) Au_7Si, and (d) Au_2Si_4, plotted by VESTA.[46]

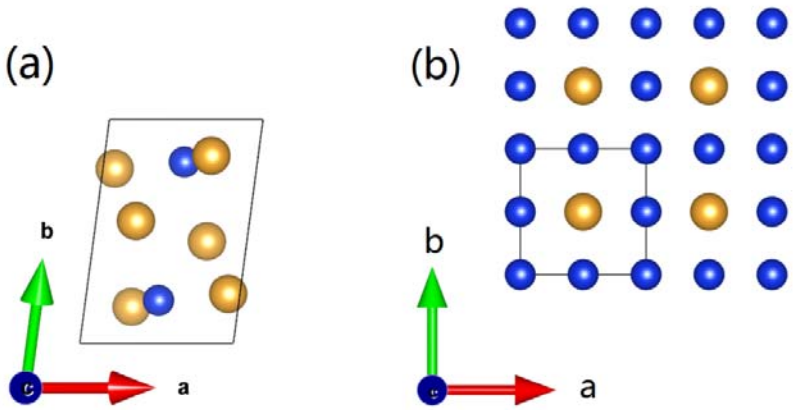

FIG. 8. Lowest-energy structures of (a) Au_6Si_2 and (b) $AuSi_7$, plotted by VESTA.[46]

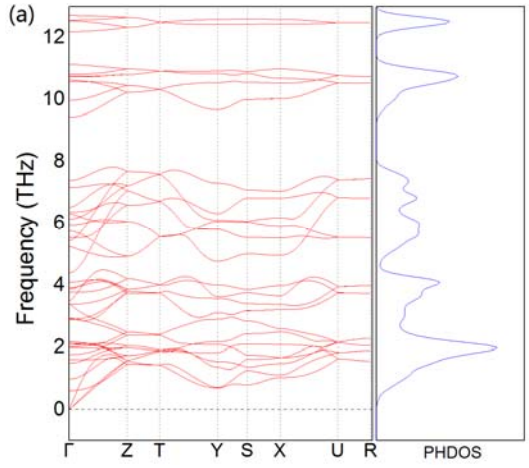
(a)
Frequency (THz)
12
10
8
6
4
2
0
Γ Z T Y S X U R
PHDOS

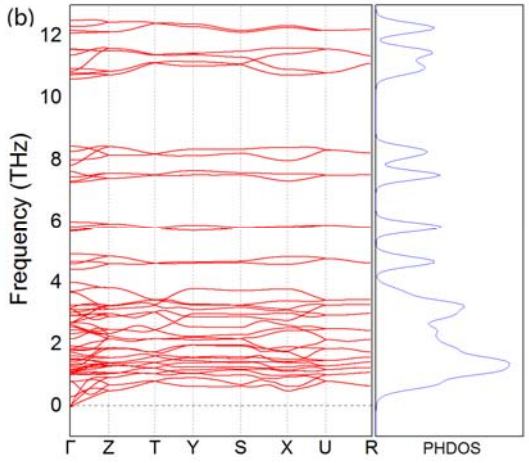
(b)
Frequency (THz)
12
10
8
6
4
2
0
Γ Z T Y S X U R
PHDOS

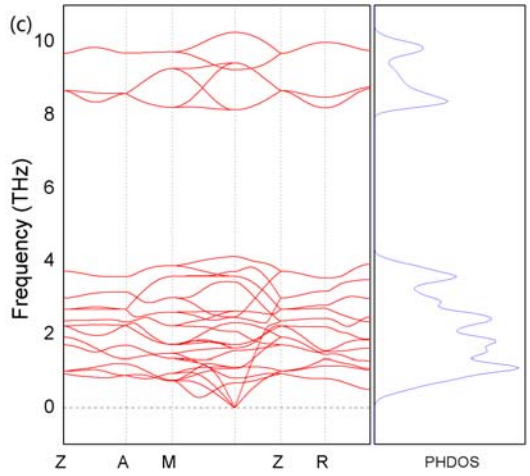
(c)
Frequency (THz)
10
8
6
4
2
0
Z A M Z R
PHDOS

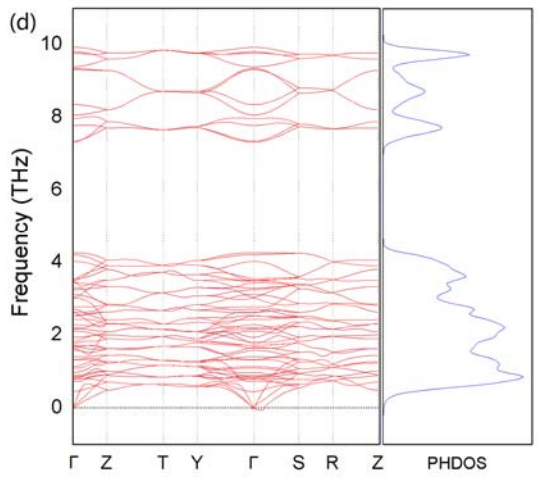

FIG. 9. Phonon band structures of the structures(a) Au_8Si_8, (b) $Au_{16}Si_8$, (c) Au_8Si_2, and (d)$Au_{16}Si_4$.

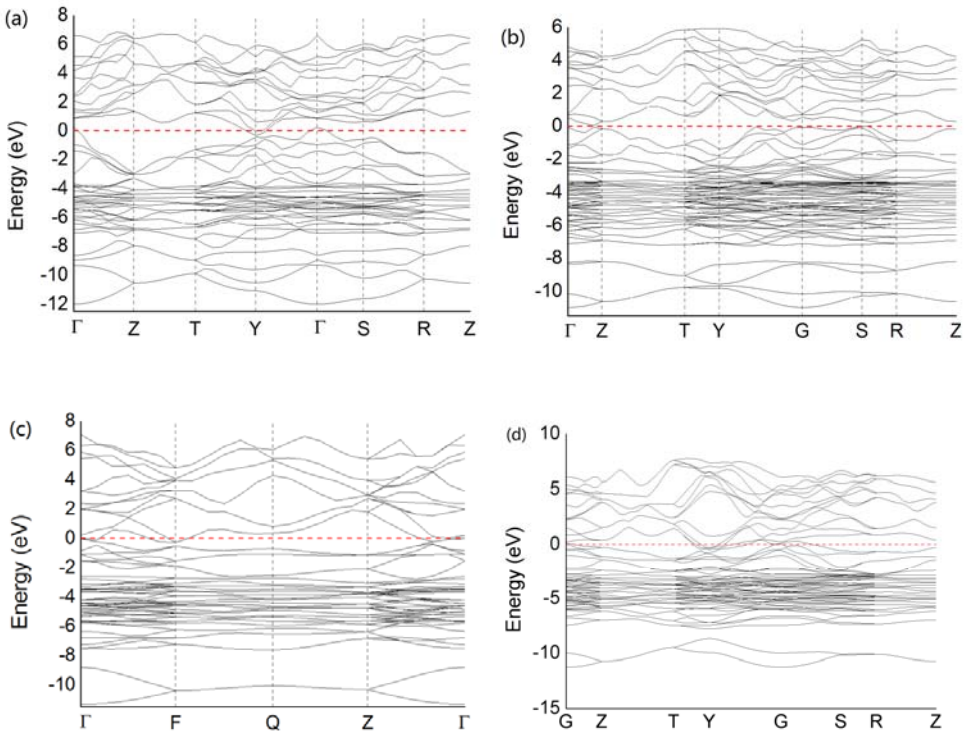

FIG. 10. Electronic band structures of the structures (a) Au_8Si_8, (b) $Au_{16}Si_8$, (c) Au_8Si_2, and (d)$Au_{16}Si_4$.

TABLE I. k-point meshes for different compositions.

Atom number	K-point meshes	Compositions
1	16 × 16 × 16	Au primitive cell
2	13 × 13 × 13	Si primitive cell
4	10 × 10 × 10	Au conventional cell, Au_3Si_1, Au_2Si_2, Au_1Si_3
5	9 × 9 × 9	Au_4Si_1, Au_3Si_2
6	9 × 9 × 9	Au_4Si_2, Au_2Si_4
7	8 × 8 × 8	Au_4Si_3
8	8 × 8 × 8	Si conventional cell (Diamond), Au_7Si_1, Au_6Si_2, Au_5Si_3, Au_4Si_4, Au_3Si_5, Au_2Si_6, Au_1Si_7
10	8 × 8 × 8	Au_8Si_2, Au_6Si_4
12	7 × 7 × 7	Au_8Si_4, Au_4Si_8
14	7 × 7 × 7	Au_8Si_6
16	6 × 6 × 6	$Au_{14}Si_2$, $Au_{12}Si_4$, $Au_{10}Si_6$, Au_8Si_8, Au_6Si_{10}, Au_4Si_{12}, Au_2Si_{14}
20	5 × 5 × 5	$Au_{16}Si_4$, $Au_{12}Si_8$
24	5 × 5 × 5	$Au_{16}Si_8$, Au_8Si_{16}

TABLE II. Optimized low-energy structures of each composition.

Au (%)	E_f(meV /atom)	Crystal system	Space group	Lattice parameter						Wyckoff site
				a	b	c	α	β	γ	
0		cubic	#227 Fd-3m	5.4307	5.4307	5.4307	90	90	90	Si:8a
12.5	87.61	tetragonal	#115 P-4m2	3.8074	3.8074	11.4187	90	90	90	Au:1b,Si2:2g,Si3:2e,Si4:1c,Si5:2g
25.0	62.21	monoclinic	#12 C2/m	5.9631	16.1414	5.0383	90	139.88	90	Au:4g Si5:8j Si6:4i
33.3	20.19	monoclinic	#12 C2/m	7.6706	5.8076	11.0254	90	150.51	90	Au:4i Si:8j
37.5	74.07	triclinic	#1 P1	4.4432	10.4919	3.8375	88.17	61.91	97.58	1a for all
50.0	-51.11	orthorhombic	#63 Cmcm	8.2745	9.3170	4.7508	90	90	90	Au:8g Si:8g
50.0	-41.94	orthorhombic	#59 Pmmn	4.725	6.794	4.875	90	90	90	Au:4e Si:4e
57.1	28.98	monoclinic	#8 Cm	5.7586	7.1564	8.5385	90	125.44	90	Au1,Au2:4b Si5,Si6,Si7:2a
60.0	13.35	triclinic	#2 P-1	4.6101	9.2177	4.5312	81.65	78.72	86.63	2i for all
62.5	15.31	triclinic	#1 P1	3.8726	7.2040	5.4341	87.01	87.91	86.52	1a for all
66.7	-32.53	orthorhombic	#20 $C222_1$	7.5076	7.2540	9.0930	90	90	90	Au1,Au2:8c, Si:8c

66.7	-21.11	orthorhombic	#33 $Pna2_1$	8.400	5.948	4.552	90	90	90	Au1,Au2:4a Si: 4a
75.0	-24.50	triclinic	#2 P-1	4.7519	6.9668	4.8389	75.56	74.51	79.11	Au1,Au2,Au4:2i Si7:2i
80.0	-29.23	tetragonal	#121 I-42m	5.761	5.761	5.549	90	90	90	Au:8i Si:2b

TABLE II (continued)

Au (%)	E_f(meV /atom)	Crystal system	Space group	Lattice parameter						Wyckoff site
				a	b	c	α	β	γ	
80.0	-28.02	orthorhombic	#20 $C222_1$	7.881	5.977	7.928	90	90	90	Au1,Au2:8c Si:4a
87.5	12.49	monoclinic	#8 Cm	8.4497	7.4481	4.9352	90	73.86	90	Au1,Au2:4b Au3,Au5,Au6:2a Si:2a
100		cubic	#225 Fm-3m	4.0783	4.0783	4.0783	90	90	90	Au:4a

TABLE III. Bader charges of Au and Si of the Au_8Si_8, $Au_{16}Si_8$, Au_8Si_2 and $Au_{16}Si_4$ structures.

Composition		Au1 (|e|/atom)	Au2 (|e|/atom)	of Si (|e|/atom)
50.00% Au	Cmcm Au_8Si_8	-0.684000		0.684000
66.67% Au	$C222_1$ $Au_{16}Si_8$	-2.120700	-0.276200	2.396950
80.00%Au	I-42m Au_8Si_2	-0.186325		0.745400
80.00% Au	$C222_1$ $Au_{16}Si_4$	0.34722	-0.18486	-0.34676

Figure captions

FIG. 1. Formation energies (E_fs) of the predicted Au-Si structures at various Au contents. The blue square and purple triangles represent the lowest-energy and the second lowest-energy structures, respectively.

FIG. 2. Lowest-energy structure of Au_8Si_8, plotted by VESTA.[46] (a) and (b) Top and side views of the Au_8Si_8 structure; (c) and (d) top view of layers #1 and #2.

FIG. 3. Top and side views of the low-energy structure of Au_4Si_4, plotted by VESTA.[46]

FIG. 4. Low-energy structures of Au_8Si_2 and $Au_{16}Si_4$, plotted by VESTA.[46] (a) and (b) Top and side views of the Au_8Si_2 structure. (c) and (d) Top and side views of the $Au_{16}Si_4$ structure.

FIG. 5. Lowest-energy structure of $Au_{16}Si_8$, plotted by VESTA.[46] (a) and (b) Top and side views of $Au_{16}Si_8$; (c) and (d) top and side views of $Au_{16}Si_8$ with normal Au atoms and cross marked Au atoms, which indicates two different 8c Wyckoff positions.

FIG. 6. Lowest-energy structure of Au_8Si_4, plotted by VESTA.[46]

FIG. 7. Lowest-energy structures of (a) Au_6Si_4, (b) Au_5Si_3, (c) Au_7Si, and (d) Au_2Si_4, plotted by VESTA.[46]

FIG. 8. (a) Lowest-energy structures of (a) Au_6Si_2 and (b) $AuSi_7$, plotted by VESTA.[46]

FIG. 9. Phonon band structures of the lowest-energy structures of (a) Au_8Si_8, (b) $Au_{16}Si_8$, and (c) Au_8Si_2. The bands were plotted in black except one that has a very small negative value plotted in red.

FIG. 10. Electronic band structures of the lowest-energy structures of (a) Au_8Si_8, (b) $Au_{16}Si_8$, and (c) Au_8Si_2.